

GT2019-90163

## RADIAL INFLOW TURBINE GEOMETRY GENERATION METHOD USING THIRD ORDER BEZIER CURVES FOR BLADE DESIGN

**U. Caldiño-Herrera**

Universidad Autónoma de Ciudad Juárez  
Ciudad Juárez, Chihuahua, México

**J.C. García**

Universidad Autónoma del Estado de Morelos  
Cuernavaca, Morelos, México

**F. Sierra-Espinosa**

Center For Research & Applied  
Sciences  
Cuernavaca, Morelos, México

**JO Dávalos**

Universidad Autónoma de  
Ciudad Juárez  
Ciudad Juárez, Chihuahua,  
México

**M. A. Lira**

Universidad Autónoma de  
Ciudad Juárez  
Ciudad Juárez, Chihuahua,  
México

### ABSTRACT

Radial inflow turbines offer larger efficiency performance for small power applications due to its geometric configuration in which flow varies its radial position along the flow path.

The geometry configuration of radial-inflow turbines demands a careful and adequate design of the flow path, since a 90° change of direction occurs from the radial inflow to the axial outflow. The blade camberline also requires attention since it defines the tangential flow direction along the meridional coordinate and any variation in its geometry affects the turbine performance.

In this paper, a method for meridional profile and camberline geometry generation is proposed and tested through CFD. The method consists in using fourth order Bezier curves for defining the hub, shroud and mid-height blade meridional profile and third order Bezier curves for defining the relative flow velocity angle along the meridional coordinate, which leads to the camberline angular position in the rotor considering radial fibered blades. The blade thickness is set to vary linearly along the meridional coordinate and along the blade height. Different configurations of blade geometry are proposed and analyzed. These configurations are fixed to satisfy the design parameters.

The code is programed in Python and adjusts the geometry data in files that are readable by meshing software. Thereby numerical calculations are performed to verify which configuration of camberline results in better performance. The calculations are done in models with the same boundary conditions and geometric data except for the variation of relative flow velocity angle along the meridional coordinate but setting the inlet and outlet angle to a fixed value. This way, the most

suitable camberline geometry can be selected. The CDF model used for this analysis was validated with the experimental results reported by Kang et al. [1]

### NOMENCLATURE

$A$	Flow area
$b$	Blade height
$C$	Absolute velocity
$D_s$	Specific diameter
$h$	Enthalpy
$L_z$	Rotor axial length
$r$	Radius
$t$	Blade thickness
$m$	Meridional coordinate
$\dot{m}$	Mass flow rate
$N_R$	Number of blades
$N_s$	Specific speed
$P$	Anchor points for Bezier curves
$U$	Blade velocity
$z$	Axial direction
$\alpha$	Absolute velocity angle
$\beta$	Relative velocity angle
$\eta$	Efficiency
$\rho$	Density
$\theta$	Blade angular position
$\omega$	Rotational speed

## Subscripts

<i>blk</i>	Blockage
<i>h</i>	Hub
<i>in</i>	Rotor inlet
<i>out</i>	Rotor outlet
<i>t</i>	Blade tip
<i>s</i>	Isentropic condition
<i>0</i>	Stagnation condition

## INTRODUCTION

Radial inflow turbines had been used widely for low power applications such as turbocharging [1, 2], Organic Rankine cycle [3, 4, 5] and nuclear facilities [6] among others. The wide use of this type of turbomachines is due its simplicity, reliability, fast response and low emissions.

Geometric configuration of radial inflow turbines is an important step during the design process, since the fluid dynamics effects on turbine performance is widely affected by this factor. Thereby, the study of isentropic performance in radial inflow rotors had been attended by different researchers [7, 8].

Many designs methodologies had been proposed looking to achieve an efficient turbine considering the rotor geometry [9, 10, 11]. Nevertheless, the performance along the rotor varies according to the thermodynamic variables, the kinematic parameters and the geometric conditions. Therefore, an evaluation of the turbine efficiency loss along the rotor is mandatory to identify the geometric, kinematic and thermodynamic conditions that causes energy losses.

The variation of turbine efficiency along the rotor had been studied by Song et al. These researchers developed a method for analyzing ORC turbine's efficiency from the preliminary design (1D method) through velocity triangles and loss models [12] considering a variable turbine efficiency and using a loss model based on air radial turbines performance. Their results were focused on the thermodynamic and kinematic influence in the variation of isentropic efficiency.

In this paper, the geometry generation of a radial inflow turbine for an ORC application is calculated and analyzed through CFD. The geometry generation starts from a preliminary design which allow to know the general dimensions of the rotor (inlet diameter, axial length, outlet blade hub and shroud radius and relative flow directions). These dimensions are calculated so flow continuity and thermodynamic conditions at inlet and outlet are fulfilled. The meridional curves are defined by fourth order Bezier curves and the blade camberline is defined by third order Bezier curves using the relative velocity direction at inlet and outlet as first and last anchor points

## ROTOR DESIGN

To generate the 3D rotor geometry the general dimensions of the rotor must be calculated. Thereby, preliminary design calculations are performed. Once these values are calculated, the meridional profiles at hub and shroud are calculated through 4<sup>th</sup> order Bezier curves. The blade camberline is defined through 3<sup>rd</sup> order Bezier curves using different configurations of anchor

points but maintaining fixed the first and last point, which correspond to the inlet and outlet relative velocity direction. Finally, a numerical analysis of the flow inside the rotor is performed using the boundary conditions calculated in the preliminary design. From this analysis, the best configuration is selected considering the thermodynamic performance of rotor. The methodology is divided in 3 stages: preliminary design, geometry generation and CFD analysis. A detailed description of each one of these stages is shown below.

## Preliminary design

This case of study demands a radial inflow turbine to produce a power output of 10 kW using R245fa as working fluid and a mass flow rate of 0.678 kg/s. The inlet temperature and pressure are 333.12 K and 4.365 bar respectively and the outlet pressure is set to be 1.59 bar. These inlet parameters are shown in Table 1 and were calculated from the thermodynamic analysis of the ORC, in which the most suitable operating conditions were found for the specific energy source available for the Organic Rankine Cycle (solar radiation from the central region of Mexico). Thereby the turbine design must adjust to these operating conditions.

Table 1. Input parameters for preliminary design

Property	Value	Units
<b>Inlet temperature</b>	333.12	K
<b>Inlet pressure</b>	4.365	Bar
<b>Outlet pressure</b>	1.59	bar
<b>Power output</b>	10	kW
<b>Mass flow rate</b>	0.678	kg/s
<b>Working fluid</b>	R245fa	-

Preliminary design consists on defining the general rotor dimensions by comparing the kinematic conditions, the thermodynamic properties and the geometric dimensions so all of them fit to satisfy the continuity condition described by Eq. (1). Continuity condition must be satisfied along the entire flow path in the rotor. Thereby, for preliminary design purposes, this equation is computed at rotor inlet and outlet.

$$\dot{m} = \rho C_m A \quad (1)$$

The left side of Eq. (1) is the mass flow rate, which is an input parameter for the design. In the right-hand side, the first term corresponds to density, and it is calculated from the equation of state of the working fluid. The second term is the meridional velocity of the fluid, i.e. the velocity component normal to the flow area at inlet and outlet respectively. To compute this value, the velocity triangle is required and therefore, defining the blade velocity  $U$ , and the absolute and relative velocity directions is mandatory.

Blade velocity is defined by rotational speed, which is computed from the adimensional number  $N_s$  defined as follows:

$$N_s = \frac{\omega \sqrt{\frac{\dot{m}}{\rho}}}{\Delta h_0^{0.75}} \quad (2)$$

For this work  $N_s$  is set to be 0.657 so a rotational speed of 2907.01 rad/s is obtained. The blade velocity is then calculated by its radial position on the rotor. This value is computed from the adimensional number  $D_s$ , defined as:

$$D_s = \frac{D_{in} \Delta h_0^{0.25}}{\sqrt{\frac{\dot{m}}{\rho}}} \quad (3)$$

According to Baines et al. [10] the product of  $N_s$  and  $D_s$  must be close to 2. It is also recommended by Baines et al. and Dixon [13] to use an inlet relative velocity angle  $\beta$  between  $-40^\circ$  and  $-20^\circ$ . An algebraic analysis reveals that negative relative velocity angles only occurs for values of  $N_s D_s$  greater than 2 as shown in Figure 1.

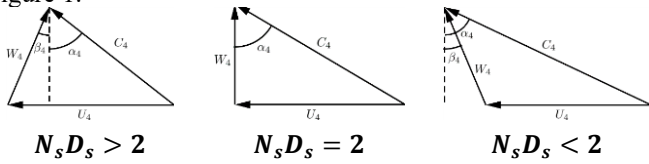


Figure 1. Velocity triangles according to  $N_s D_s$

Thereby,  $N_s D_s$  is set to be 2.3 and now blade velocity can be calculated. The tangential component of the absolute velocity is calculated from the Euler equation for turbomachinery considering a purely axial absolute velocity at rotor outlet. This way the kinematic conditions are calculated. Finally, the geometric conditions need to be defined to satisfy the continuity conditions in Eq. (1). The flow surface at inlet is defined by Eq. (1)

$$A_{in} = 2\pi r_{in} b_{in} - A_{blk_{in}} \quad (4)$$

Where the first term of the right had side corresponds to the surface of a cylindrical shell of radius  $r_{in}$  and height  $b_{in}$  and the second term corresponds to the blockage produced by the blades at this region, which is defined by the number of blades  $N_R$  and the blade height  $b$  and thickness  $t$ . For this work, the thickness of the blade is constant at rotor inlet and varying with a linear behavior as meridional direction increases. This linear behavior is set to be greater for thickness at tip than thickness at hub. In this work, the subscript *in* and *out* refers to the inlet and outlet respectively and the subscripts *h* and *t* refers to the hub and tip of the blade respectively.

$$A_{blk_{in}} = N_R b_{in} t_{in} \quad (5)$$

$$t_{in} = 0.04 r_4 \quad (6)$$

Where,  $N_R$  is the number of blades in the rotor. This value is calculated through the relation given by Rohlik [3] which is shown in Eq. (7).

$$N_R = \frac{\pi}{30} (110 - \alpha_{in}) \tan \alpha_{in} \quad (7)$$

The flow surface at rotor outlet corresponds to an annular section minus the blockage surface produced by the blade thickness in this region.

$$A_{out} = \pi (r_{out_t}^2 - r_{out_h}^2) - A_{blk_{out}} \quad (8)$$

$$A_{blk_{out}} = N_R \left( \frac{\left( \frac{t_{out_h}}{\cos \beta_{out}} - \frac{t_{out_t}}{\cos \beta_{out}} \right) (r_{out_t} - r_{out_h})}{2} \right) \quad (9)$$

$$t_{out_h} = 0.02 r_4 \quad (10)$$

$$t_{out_t} = 0.01 r_4 \quad (11)$$

The blockage surface is calculated as the surface of a trapeze projected on an oblique plane located at an angle of  $\beta_{out}$  respect to the direction of the flow at rotor outlet as it is shown in Figure 2.

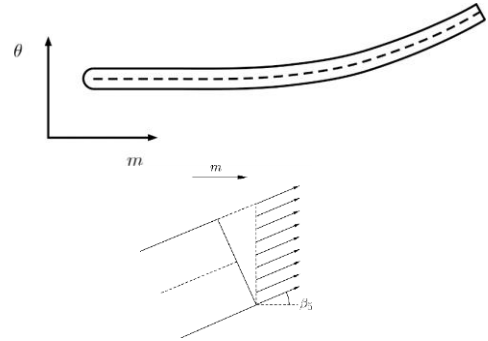


Figure 2. Blockage surface produced by a single blade

From the geometric definition of the flow surfaces, the thermodynamic conditions and some kinematic considerations such as using adimensional numbers such as specific speed  $N_s$ , specific diameter  $D_s$ , ratio between blade tip and hub height at outlet  $\lambda$  and ratio between meridional velocities at inlet and outlet  $\xi$ , the general rotor dimension are calculated as follows:

$$b_{in} = \frac{\dot{m}}{C_{m_{in}} \rho_{in} (2\pi r_{in} - N_R t_{in})} \quad (12)$$

$$r_{out_t} = \frac{N_R \left( \frac{t_{out_h}}{\cos \beta_{out}} - \frac{t_{out_t}}{\cos \beta_{out}} \right) (\lambda - 1)}{4\pi(\lambda^2 - 1)} \quad (13)$$

$$\sqrt{\frac{(\lambda - 1) \left( N_R^2 \left( \frac{t_{out_h}}{\cos \beta_{out}} - \frac{t_{out_t}}{\cos \beta_{out}} \right)^2 (\lambda - 1) + 16A_{out}\pi(\lambda + 1) \right)}{4\pi(\lambda^2 - 1)}}$$

Using the value of  $\lambda$  it is possible to calculate  $r_{out_h}$ . The blade height at turbine outlet is then calculated, and following the recommendation made by Aungier [11], the axial length of the rotor is calculated as follows.

$$r_{out_h} = \lambda r_{out_t} \quad (14)$$

$$b_{out} = r_{out_t} - r_{out_h} \quad (15)$$

$$L_Z = 1.5b_{out} \quad (16)$$

Finally, the relative velocity direction is defined as:

$$\beta_{out} = \text{atan} \left( \frac{U_{out}}{\xi C_{m_{out}}} \right) \quad (17)$$

### Geometry generation

Once the general dimensions were defined by the preliminary design, the meridional profiles and the camberline geometry are calculated. The meridional profiles define the hub and shroud positions along the meridional coordinate, i.e. the radial position of the blade hub and tip along the axial coordinate. The camberline is the azimuthal position of the blade within the rotor along the axial coordinate and it is associated with the fluid relative velocity direction as it moves along the rotor. Combining the camberline angular position ( $\theta$ ) with the meridional profile at different blade heights ( $r, z$ ) results in the complete 3D geometry for the rotor for one flow channel (single blade and periodic lateral walls).

### Meridional profile

Hub and shroud meridional profiles are defined through 4<sup>th</sup> order Bezier curves. A third meridional profile is also calculated, which corresponds to the mid height blade coordinate. This last meridional profile is used to calculate the camberline coordinates in the following subsection but its calculated in this stage of the design process. Figure 3 shows schematically the anchor points for hub and shroud and Table 2 shows the values associated to the anchor points for each meridional profile. Using the anchor points as shown in Table 2 ensure a smooth and descending change in the  $r$  position, which is mandatory in the fluid direction transition from radial-inflow to axial-outflow.

The meridional profile lies on the plane ( $r, z$ ) so Bezier functions for  $z$  and  $r$  are calculated for each meridional profile through Eq. (18).

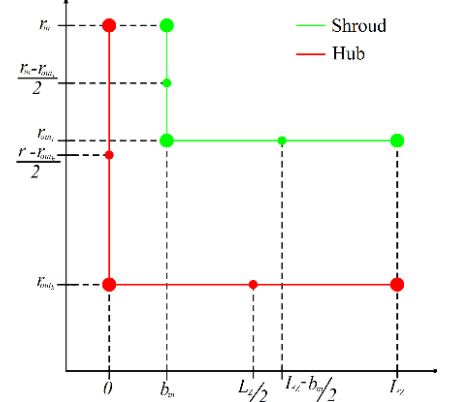


Figure 3. Anchor points for meridional profiles at hub and shroud

The radial position of the meridional curve at mid-height is required for evaluating the angular coordinate of the blade at this constant span value since radial fibered blades were selected for the turbine. Thereby, for each meridional profile there is a 4<sup>th</sup> order polynomial function that defines its position along the  $m$  coordinate according to Eq. (18).

$$B(m) = P_0(1 - m)^4 + 4P_1m(1 - m)^3 + 6P_2m^2(1 - m)^2 + 4P_3m^3(1 - m) + P_4m^4 \quad (18)$$

### Camberline

The camberline is the geometric region that imposes the fluid direction within the rotor as it flows along the meridional coordinate. The change in the direction of the fluid is necessary so the Euler equation could be satisfied. From the preliminary design, the fluid direction at inlet and outlet are known, nevertheless, the variation from  $\beta_{in}$  at  $m = 0$  to  $\beta_{out}$  at  $m = 1$  must be defined. This variation must be selected carefully due to its influence in the turbine performance. From the preliminary design, the flow direction at inlet and outlet are known. These values were calculated from the Euler equation for turbomachines and ensure that power output requirement is fulfilled. Nevertheless, the variation of  $\beta$  from inlet to outlet must be defined as a smooth transition. This condition leads to the idea of using 3<sup>rd</sup> order Bezier curves to define the variation of  $\beta$  along the normalized meridional position  $m$ . The function resulting from a 3<sup>rd</sup> order Bezier curve is a 3<sup>rd</sup> order polynomial function.

Table 2. Anchor points for meridional profiles at hub, mid-height and tip

Anchor point	Hub		Mid height		Tip	
	$z$	$r$	$z$	$r$	$z$	$r$
$P_0$	0	$r_{in}$	$0.5b_{in}$	$r_{in}$	$b_{in}$	$r_{in}$
$P_1$	0	$\frac{r_{in} + r_{out_h}}{2}$	$0.5b_{in}$	$\frac{r_{in} + r_{out}}{2}$	$b_{in}$	$\frac{r_{in} + r_{out_t}}{2}$
$P_2$	0	$r_{out_h}$	$0.5b_{in}$	$r_{out}$	$b_{in}$	$r_{out_t}$
$P_3$	$\frac{L_z}{2}$	$r_{out_h}$	$\frac{L_z + 0.5b_{in}}{2}$	$r_{out}$	$\frac{L_z + b_{in}}{2}$	$r_{out_t}$
$P_4$	$L_z$	$r_{out_h}$	$L_z$	$r_{out}$	$L_z$	$r_{out_t}$

A third order Bezier curves requires 4 anchor points, nevertheless 2 of these points are fixed:  $P_0$  corresponds to a meridional coordinate of 0 and a  $\beta$  angle of 0 and  $P_3$  corresponds to a meridional coordinate of 1 and a  $\beta$  angle of  $\beta_{out}$ . The other two points result from dividing the  $m$  coordinate and the  $\beta$  range into 3 equal parts. The combination of this anchor points results in 16 curves of  $\beta(m)$ . The anchor points of these 16 curves are shown in Table 3.

Table 3. Anchor points for 16 curves of  $\beta(m)$  for camberline definition

Curve	P1		P2	
	$m$	$\beta$	$m$	$\beta$
1	0.333	0	0.666	0
2	0.333	0	0.666	0.333
3	0.333	0	0.666	0.666
4	0.333	0	0.666	1
5	0.333	0.333	0.666	0
6	0.333	0.333	0.666	0.333
7	0.333	0.333	0.666	0.666
8	0.333	0.333	0.666	1
9	0.333	0.666	0.666	0
10	0.333	0.666	0.666	0.333
11	0.333	0.666	0.666	0.666
12	0.333	0.666	0.666	1
13	0.333	1	0.666	0
14	0.333	1	0.666	0.333
15	0.333	1	0.666	0.666
16	0.333	1	0.666	1

For radial fibered blades, the relation between the flow direction  $\beta$  and the azimuthal position of the blade within the rotor  $\theta$  is:

$$\frac{d\theta}{dm} = \frac{\tan[\beta(m)]}{r(m)} \quad (19)$$

As mentioned before, the camberline is computed for a span value of 0.5 (defined by the mid height blade meridional profile),

thereby, the denominator in the right-hand side of Eq. (19) is a 4<sup>th</sup> order polynomial function of  $m$ . For the numerator of this term, the function is the tangent of a third order polynomial function of  $m$  since  $\beta(m)$  is a 3<sup>rd</sup> order Bezier curve. To compute the values of  $\theta$  along  $m$ , the differential equation is solved numerically using the boundary condition of  $\theta(0) = 0$

Once the values of  $\theta(m)$  are known, they are combined with the values of  $(r,z)$  obtained for the mid-height meridional profile so the combination  $(r,\theta,z)$  leads to the camberline on the mid-height span. For radial fibered blades, the same values of  $\theta$  are combined with the coordinates  $(r,z)$  of the meridional profiles of hub and shroud. Linking the 3 camberlines (hub, mid, height, shroud) the blade is fully defined.

The lateral walls are generated by displacing the generated blade only on its angular coordinate a value of  $\frac{\pi}{2N_R}$  in the positive and negative direction. The hub and shroud camberlines are revolved along the  $z$  axis this same angular value to define the hub and shroud surfaces

### CFD Analysis

The geometric domain generated was discretized with a structured mesh of 1,237,680 elements and the boundary conditions were the ones shown in Table 4.

The CFD analysis was performed on Ansys CFX software using the Shear Stress Transport as the turbulence model and the Aungier-Redlich-Kwong real gas model as the equation of state. The validation of these CFD modelling conditions was done by analyzing the experimental work reported by Kang et al. [13]. For this validation, a numerical experiment was performed with the rotor geometry and the boundary conditions reported by Kang et al. and using the numerical models mentioned previously. A power output of 31.2 kWe was reported by Kang et al. and a power output of 31.7 kWe was obtained by the numerical model used in the present work. Thereby, the numerical model was considered valid to solve accurately the flow that occurs in an ORC radial-inflow turbine.

The CFD analysis was performed in the 16 geometries to evaluate the performance of each rotor. Twenty streamwise positions were evaluated at a constant span of 0.5. starting from  $m = 0$  and finishing at  $m = 1$ . On these positions, the actual enthalpy is computed using the equation of state through the total

pressure and total temperature in the corresponding point of evaluation. Also, the ideal enthalpy is computed using the equation of state and the total pressure and the rotor inlet entropy to calculate the isentropic efficiency at each one of the streamwise position using Eq. (20).

$$\eta_s = \frac{h_{0in} - h_i}{h_{0in} - h_{is}} \quad (20)$$

Table 4. Boundary conditions for the CFD analysis

Condition	Region	Value	Units
Total pressure	Inlet	4.365	bar
Total temperature	Inlet	4.365	K
Static pressure	Outlet	1.59	bar
Axial velocity component	Inlet	0	[-]
Radial velocity component	Inlet	0.34182	[-]
Tangential velocity component	Inlet	-0.93976	[-]
Rotational speed	Full domain	2907.01	rad/s
Periodicity	Lateral Walls	[-]	[-]

Where,  $h_i$  is the enthalpy on the  $i$ -th streamwise position (calculated from total pressure and total temperature in that position) and  $h_{is}$  is the ideal enthalpy on the  $i$ -th streamwise position (calculated from total pressure and rotor inlet entropy). To associate the turbine isentropic efficiency with the flow dynamics, a comparison between the relative flow direction and the calculated flow direction defined by the blade camberline is performed. This calculation is done by subtracting the actual relative flow angle resulted from the CFD calculations and the relative velocity direction defined by the beta value in the camberline definition as shown in Eq. (21)

$$\Delta\beta = \beta_{bl} - \beta_{CFD} \quad (21)$$

Where  $\beta_{bl}$  is the direction of the fluid calculated from the Bezier curve and  $\beta_{CFD}$  is the relative fluid direction obtained from the CFD calculations. Both values evaluated along the streamwise position.

## RESULTS

Using the methodology described in the previous section, the general dimensions of the rotor were calculated through the preliminary design and are shown in Table 5.

Table 5. General dimensions of the rotor

Parameter	Value	Units
$r_{in}$	45.89	mm
$b_{in}$	4.37	mm
$t_{in}$	1.8	mm
$r_{out_t}$	27.27	mm

$r_{out_h}$	10.91	mm
$t_{out_t}$	0.46	mm
$t_{out_h}$	0.91	mm
$N_R$	12	blades
$L_z$	24.54	mm
$\beta_{out}$	-51.52	°

The meridional profiles were defined by 4<sup>th</sup> order Bezier curves were plotted on a ( $r; z$ ) plane and are shown in Figure 4. The polynomial equation that defines the mid-height meridional profile (black dotted in Figure 4) is:

$$r(m) = r_{in}(1 - m)^4 + 4 \frac{r_{in} + r_{out}}{2} m(1 - m)^3 + 6r_{out}m^2(1 - m)^2 + 4r_{out}m^3(1 - m) + r_{out}m^4 \quad (22)$$

It is important to emphasize that the meridional profiles are the same for the 16 rotors. The only variable is the camberline, which is given only by the angular position along the meridional profiles.

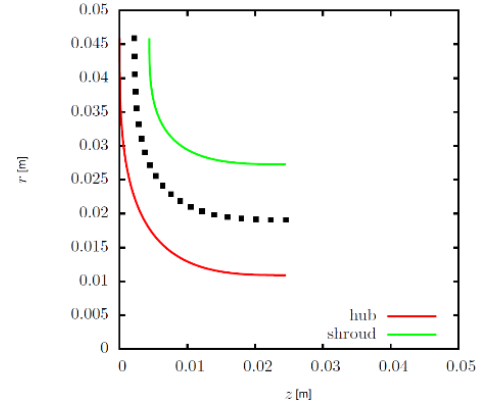


Figure 4. Hub, shroud and mid-height meridional profiles

According to the anchor points to define the variation of the relative velocity along the meridional coordinate shown in Table 3, the resulting 16 curves are plotted in Figure 5. Each one of these curves is defined by a third order Bezier curves so each one of the corresponding camberlines is calculated by solving Eq. (19).

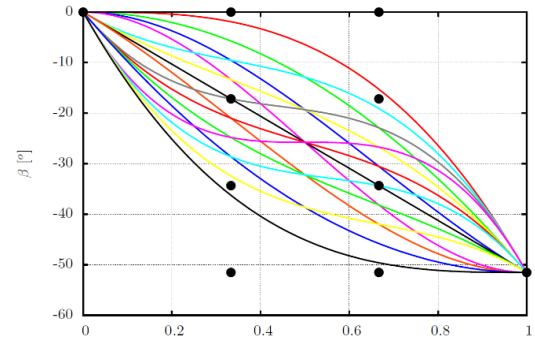


Figure 5. Variation of  $\beta$  along  $m$  coordinate (Bezier curves)

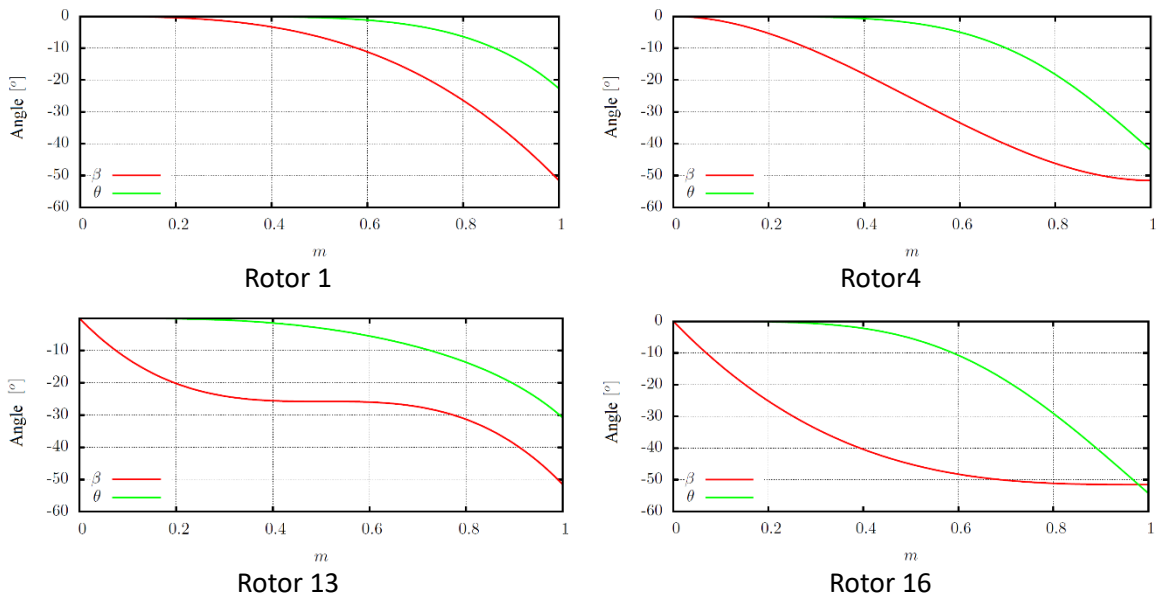


Figure 6. Camberline and relative velocity direction

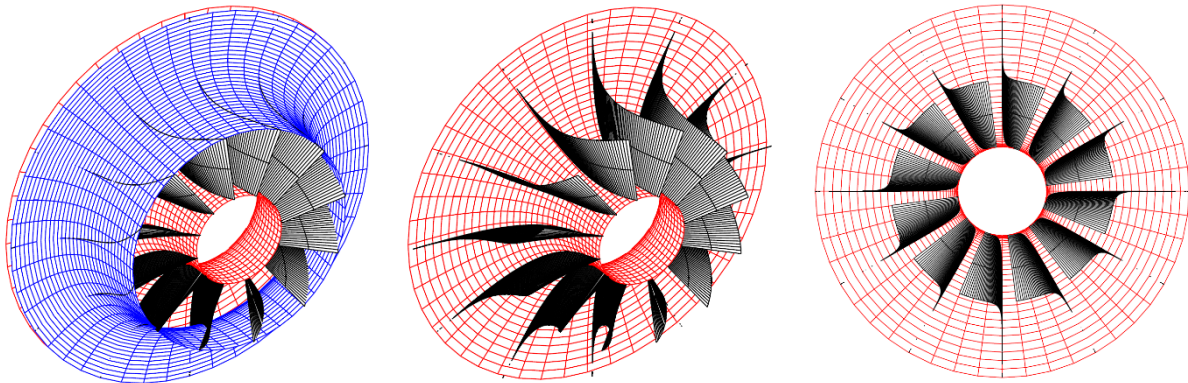


Figure 7. Generated geometry for rotor 1

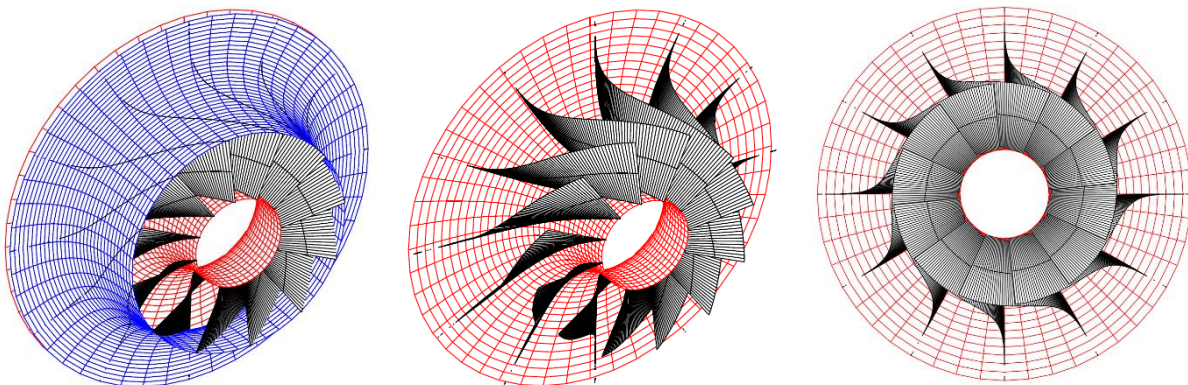


Figure 8. Generated geometry for rotor 16

The initial and final value of  $\beta$  is the same for the 16 rotor configurations as could be noticed in Figure 6. Nevertheless, the variation from  $0^\circ$  to  $-51.52^\circ$  is different for each configuration. The influence of this behavior on the camberline is shown in Figure 6. Only 4 camberlines are shown (in green) with its corresponding  $\beta$  values (in red). These 4 configurations are shown due to the geometric properties of  $\beta(m)$  so its influence on camberline could be noticed.

The full rotor geometry of rotor 1 and 16 is shown in Figure 7 and Figure 8 respectively. This figure shows an isometric view of the shrouded and unshrouded rotor, and it also shows a frontal unshrouded view in which it is clear how the blade geometry leads to a change in the direction of the working fluid.

In Figure 9, the flow channel for one blade is shown for rotor 1 and 16 respectively. The lateral walls are not shown to allow visualization of the blade. This flow channel is used as the geometric domain in which the working fluid is analyzed under the boundary conditions described in the previous section.

Applying the boundary conditions, real gas model, turbulence model and solution method defined in the previous section, the CFD analysis was performed. As a result of the numerical analysis, the flow variables such as velocity, pressure and temperature are known. These 3 variables were used to evaluate the performance of each one of the 16 rotors by comparing 2 main parameters: isentropic efficiency and relative flow deviation. For the isentropic efficiency, an evaluation of the enthalpy drop along the meridional coordinate on a constant span of 0.5 was carried out. Comparing the actual enthalpy drop (from CFD calculations) with the ideal enthalpy drop (isentropic expansion), the isentropic efficiency is computed and plotted for the 16 rotors analyzed. It is important to mention that the ideal enthalpy drop is calculated considering the rotor inlet position as the reference point, i.e. the entropy generation is considered to occur since this point. Thereby, at leading edge ( $m = 0$ ) the entropy has already increased and therefore, isentropic efficiency had decreased at this point. This information is shown in Figure 10 for the 16 rotors evaluated.

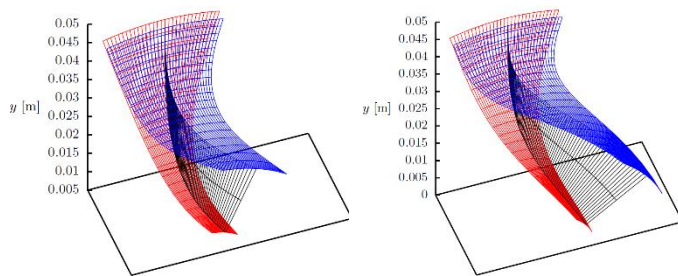


Figure 9. Flow channel for rotor 1 and 16

The flow direction attachment was calculated as the difference between the direction imposed by the camberline and the CFD calculations. This parameter is shown in Figure 11 for the 16 rotors analyzed. It is important to mention that for the 16

configurations analyzed, the actual flow direction at inlet is  $30^\circ$ , meanwhile, the blade inlet angle was set to  $0^\circ$ .

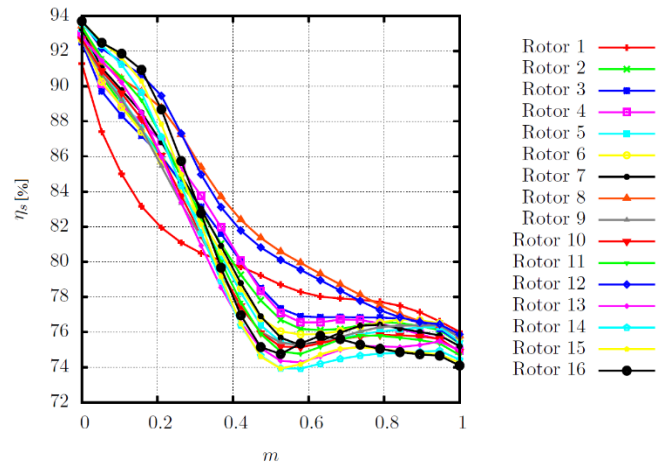


Figure 10. Isentropic efficiency variation along the rotors

Thereby, the flow tends to attach to the blade direction as it moves along the rotor. The reason for this difference is as follows: the flow in radial-inflow turbines shows bet attachment to the blade direction when the relative velocity inlet direction is not radial, but has a direction between  $-20^\circ$  and  $-40^\circ$  with respect to the radial direction [10], on the other hand, to minimize mechanical stress conditions on the blades, radial fibered blades are recommended, ths blades require to have an inlet relative angle of  $0^\circ$  with respect to the radial direction [10, 11]. It exists a close relation between the efficiency lost and the non-attachment condition in the actual flow with the design dircion defined by  $\beta_{bl}$ .

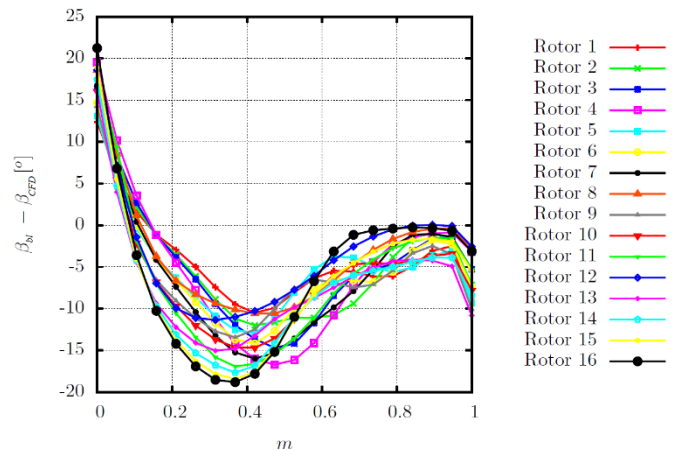


Figure 11. Variation of the actual flow direction and the flow direction imposed by the blade

The total efficiency for each rotor configuration is shown in Table 6. The values in this table correspond to the isentropic efficiency of the rotor at  $m=1$ . Although the isentropic efficiency does not varies beyond 1% between the lowest and highest efficiency, the variation of this parameter along the meridional



coordinate leads to define regions associated with camberline configuration in which isentropic efficiency drop is minimum.

Table 6. Turbine isentropic efficiency for the 16 rotor configurations

Rotor	Efficiency [%]	Rotor	Efficiency [%]
1	76.013	9	75.673
2	75.344	10	74.888
3	75.393	11	74.688
4	74.910	12	75.866
5	75.465	13	74.945
6	75.729	14	74.424
7	75.196	15	74.257
8	75.788	16	74.089

To evaluate the flow attachment to the blade, the total deviation is computed as the area under the curve of the variation of the flow deviation along the meridional coordinate for each rotor. This area is defined as the sum of absolute values, since a positive deviation and a negative deviation affects in the same manner the development of the flow for this analysis purposes. Figure 12 shows schematically how this value is calculated for rotor 1.

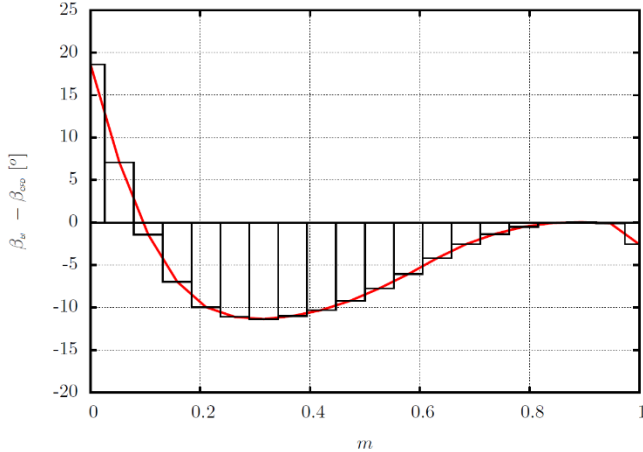


Figure 12. Flow attachment quantification by area under the curve

The total flow deviation of the 16 rotors analyzed are shown in Table 7. It is expected that the lower the flow deviation, the larger the efficiency loss in each rotor. It is noticed that it exists a close relation between the flow behavior associated with the attachment of the actual direction with the blade direction and the efficiency drop along the meridional coordinate since rotor 1 is the rotor that shows the lowest deviation and the highest efficiency.

Table 7. Flow deviation for the 16 rotor configurations

Rotor	Deviation [°]	Rotor	Deviation [°]
1	175.95	9	216.30
2	191.98	10	224.15
3	195.67	11	233.48
4	215.80	12	177.39
5	193.90	13	243.92
6	202.57	14	254.17
7	214.78	15	241.10
8	178.20	16	230.18

## ANALYSIS AND DISCUSSION

According to the results presented in the previous section, the isentropic efficiency varies in different forms from one rotor to another. Nevertheless, the variation differs from one rotor to another. Figure 10 shows how rotor 1 presents a quick drop on turbine efficiency (9.334%) compared to the rest of the analyzed rotors in the range of  $0 \leq m \leq 0.2$ . Nevertheless, for the range  $0.2 \leq m \leq 1$  the efficiency drop is 5.931%. On the other hand, for rotors 12 and 16 in the range  $0 \leq m \leq 0.2$ , the efficiency drop is 4.227% and 5.931% respectively and in the range of  $0.2 \leq m \leq 1$  is 13.585% and 14.59%.

These 3 rotors are mentioned since rotor 1 showed the highest isentropic efficiency, nevertheless, in the range of  $0.2 \leq m \leq 1$  the efficiency drop is the largest among the 16 rotors analyzed. On the other hand, rotor 12 and 16 showed the lowest efficiency drop in the range of  $0 \leq m \leq 2$  and specifically rotor 16 resulted in the lowest final isentropic efficiency. Rotor 12 was the second largest efficiency just below rotor 1.

This leads to associate efficiency drop rate in the rotor with the camberline configuration. As it is noticed in Figure 6, regardless the behavior of  $\beta(m)$ , the camberline curve  $\theta(m)$  shows as similar behavior with a slope going from 0 to a negative value, increasing the magnitude of the slope as  $m$  increases. The main difference in the 16 camberlines is the final angular position. For rotor 1, the final angular position is  $21.5^\circ$  and for rotor 16 the final angular position is  $54.2^\circ$ . Figure 7 and Figure 8 show on the frontal view how rotor 1 require a smaller turn in the blade to achieve the final velocity direction  $\beta$ , whereas rotor 16 require a larger turn in the blade to achieve the same final velocity direction.

This condition is due to the variation of  $\beta$  along  $m$ . For example, rotor 1 shows a mainly constant behavior for  $0 \leq m \leq 0.2$ , which results in a large efficiency drop. Meanwhile, rotor 16 in the same range of  $m$  shows a non-linear decreasing behavior for  $\beta(m)$  and this results in a low efficiency drop. On the other hand, rotor 1 in the range of  $0.6 \leq m \leq 1$  shows decreasing non-linear behavior for  $\beta(m)$  and this results in a low efficiency drop, and rotor 16 shows a mainly constant value of  $\beta$  for the same range of  $m$ , which results in a low value of efficiency drop. This means that not only the variation of  $\beta(m)$  affects the efficiency drop, but the meridional position in which this variation occurs,

since a mainly constant  $\beta$  at turbine inlet results in larger efficiency drop and a mainly constant  $\beta$  at turbine outlet results in lower efficiency drop.

In regards the flow deviation, it exists consistency between its influence in the efficiency loss along the rotor. Thereby, a relation could be inferred between these 2 performance parameters. Since the data was collected in only 20 points along the meridional coordinate, some variation exists. The major differences in consistency between these 2 parameters occurs with rotor 2 which in terms of efficiency is placed in the 8<sup>th</sup> position while in terms of flow deviations is the 4<sup>th</sup> place. As mentioned previously, the discrepancy is due to the large meridional step used for the calculation in the area under the curve. Thereby, a smaller meridional step will lead to more accurate results.

## CONCLUSIONS AND RECOMMENDATIONS

The geometry generation method proposed in this paper allows to define the fluid domain used for the CFD analysis. Since the method defines the meridional profiles and the variation of the velocity direction through Bezier curves, the camberline can be computed by solving a differential equation than involves polynomial functions.

Once the CFD analysis is complete, an evaluation of the isentropic efficiency was performed, and it was possible to evaluate the efficiency drop along the rotor meridional coordinate. The efficiency drop is then compared with the camberline angular position on the rotor and with the actual flow velocity direction to identify the kinematic-geometric conditions which lead to minimize the efficiency drop. It was observed that the more a camberline turns (increases the angular position on the rotor) the more the efficiency drops. For rotor 1, a turbine efficiency of 76.013% was obtained with final blade angular position  $\theta$  of 21.15°. Meanwhile, rotor 16 resulted in an isentropic efficiency of 74.089% with a final blade angular position of 54.2°. Thereby, an increase of 1.924% in isentropic efficiency is obtained by this rotor geometry generation method.

The flow deviation between the CFD calculations and the proposed blade geometry showed a close connection with the isentropic efficiency. This connection implies that as lower the flow deviation (the area under the curve in the graph of flow deviation and the meridional coordinate), the lower the efficiency drop and thereby a better performance is achieved. To ensure this connection, it is recommended to use a smaller meridional step during the calculations of flow deviation in the CFD results, since the results presented in this work only considered a discretization in 20 equidistant points.

The main recommendation is to perform experimental tests for the operation of the radial-inflow turbine. Thereby, a testing bench with pump, evaporator and condenser is required for the experimental tests. With the experimental data, the CFD models used for this case of study (ORC turbine) will be strengthened. Therefore, numerical experiments could be performed considering piecewise functions since certain variations of  $\beta$  in certain  $m$  ranges lead to lower efficiency drop. Thereby, selecting the conditions that resulted in lower efficiency drop and

putting them together could result in a higher isentropic efficiency, which is a very important issue on ORC systems where thermal efficiency is low by default since the temperature difference within the cycle is small (lesser than 60 K).

The result of these numerical calculations could also be introduced into a neural network that will lead to the optimum camberline geometry using the anchor points as output variables and isentropic efficiency or flow deviation as objective function. Thereby, a second recommendation is to use neural networks for finding the optimal geometric conditions for the ORC turbine.

## ACKNOWLEDGMENTS

The main author would like to thank Science and Technology Nacional Council (CONACyT) for the economic support on his graduate studies (grant number 384084) which lead to the development of this work.

## REFERENCES

- [1] R. Harald, G. Marc and B. Martin, "Computational Fluid Dynamics Analysis of a Radial Turbine During Load Step Operation of an Automotive Turbocharger," *Journal of Fluids Engineering*, vol. 140, no. 2, 2017.
- [2] B. Fabio and D. B. Vincenzo, "Steady Modeling of a Turbocharger Turbine for Automotive Engines," *Journal of Engineering for Gas Turbines and Power*, vol. 136, no. 1, 2013.
- [3] A. Meroni, M. Robertson, R. Martinez-Botas and F. Haglind, "A methodology for the preliminary design and performance prediction of high-pressure ratio radial-inflow turbines," *Energy*, vol. 164, pp. 1062-1078, 2018.
- [4] G. Lv, J. Yang, W. Shao and X. Wang, "Aerodynamic design optimization of radial-inflow turbine in supercritical CO<sub>2</sub> cycles using a one-dimensional model," *Energy Conversion and Management*, vol. 165, p. 827–839, 2018.
- [5] D. Fiaschi, G. Manfrida and F. Maraschiello, "Thermofluid dynamics preliminary design of turbo-expanders for ORC cycles," *Applied Energy*, vol. 97, pp. 601-608, 2012.
- [6] W. Bo and T. Rui-feng, "The thermodynamic design of the radial inflow nuclear turbine," in *Proceedings of the 2017 25th International Conference on Nuclear Engineering*, Shanghai, China, 2017.
- [7] J. A. C., "Design and Test of a Small, High Pressure Ratio Radial Turbine," *Journal of Turbomachinery*, vol. 118, pp. 632-370, 1996.
- [8] H. I., H. H. P. and H. S. H., "The Design and Testing of a Radial Flow Turbine for Aerodynamic Research," *Journal of Turbomachinery*, vol. 114, pp. 411-418, 1992.
- [9] M. S. Y. Ebaid, F. S. Bhinder and G. H. Khdairi, "A Unified Approach for Designing a Radial Flow Gas Turbine," *Journal of Turbomachinery*, vol. 125, pp. 598-606, 2003.
- [10] H. Moustapha, M. F. Zelesky, N. C. Baines and D. Japikse, *Axial and Radial Turbines*, Concepts NREC, 2006.

- [11] R. H. Aungier, Turbine Aerodynamics, Axial flow and radial-inflow turbine design and analysis, New York: ASME PRESS, 2005.
- [12] S. Jian, G. Chun-wei and R. Xiaodong, "Influence of the radial-inflow turbine efficiency prediction on the design and analysis of the Organic Rankine Cycle (ORC) system," *Energy Conversion and Management*, vol. 123, pp. 308-316, 2016.
- [13] S. H. Kang, "Design and preliminary tests of ORC (organic Rankine cycle) with two-stage radial turbine," *Energy*, vol. 96, pp. 142-154, 2016.
- [14] S. L. Dixon and C. A. Hall, Fluid Mechanics, Thermodynamics of Turbomachinery, Elsevier, 2010.
- [15] H. E. Rohlik, "Analytical determination of radial inflow turbine design geometry for maximum efficiency," NASA, Lewis Research Center, 1968.
- [16] S. Han, J. Seo and B.-S. Choi, "Development of a 200 kW ORC radial turbine for waste heat recovery," *Journal of Mechanical Science and Technology*, vol. 28, no. 12, pp. 5231-5241, 2014.